Materials and Design 169 (2019) 107684

Contents lists available at ScienceDirect

Materials and Design

journal homepage: www.elsevier.com/locate/matdes

Method of enhancing interlayer bond strength in construction scale 3D printing with mortar by effective bond area amplification

Taylor Marchment [a,*], Jay Sanjayan [b,c], Ming Xia [a]

[a] Centre for Sustainable Infrastructure, Faculty of Science, Engineering and Technology, Swinburne University of Technology, Hawthorn, Victoria, Australia
[b] Centre for Sustainable Infrastructure, Swinburne University of Technology, Hawthorn, Australia
[c] China University of Mining and Technology, Xuzhou, Jiangsu, China

HIGHLIGHTS

- The application of a cementitious "glue" paste between layer depositions increases bond strength up to 60%.
- Effective bond area was obtained by adding colour pigments to printed layers and image analysis of fractured interlayers.
- Effective bond area was found to have strong correlation to bond strength of the interlayer.
- Pastes containing a superplasticiser or retarder provide the largest increase in bond strength.

GRAPHICAL ABSTRACT

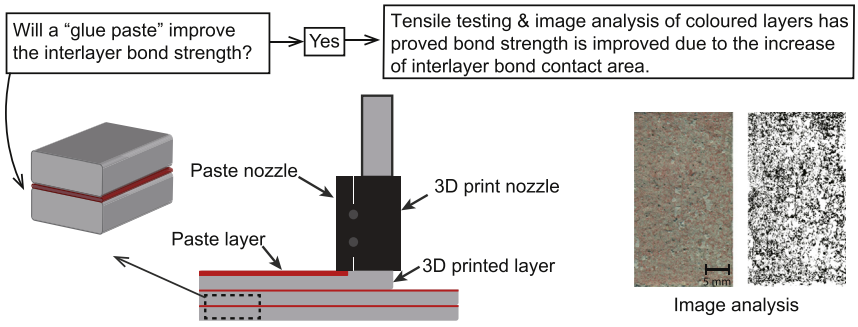

ARTICLE INFO

Article history:
Received 30 November 2018
Received in revised form 28 February 2019
Accepted 28 February 2019
Available online 01 March 2019

Keywords:
3D concrete printing
Interlayer bond
Additive manufacturing
Image analysis
Bond area

ABSTRACT

3D Construction Printing (3DCP) is a new and emerging technology that is set to revolutionise construction. Currently the technology is in its early stages of development and many hurdles are yet to overcome. Particularly in the field of extrusion 3DCP with cementitious materials, one of the primary hurdles is the weak interface bonds. The weakness in bonds is hypothesised to be present due to the layered fabrication of a stiff cementitious mix that creates a localised void structure. Due to the time gap intervals between depositions, the bond strength decreases due to lack of intermixing. This paper seeks to explore a method to strengthen the interlayer bonds, by applying a cementitious paste at the interface, to minimise voids and promote bond area. Using a flatbed scanner and a unique method of image processing on printed colour layers, a quantitative evaluation of the contact area, "effective bond" area, was determined. The application of these experimental and analytical methods shows that an increase in bond strength is achieved, which is proportional to the effective bond area.

1. Introduction

3D Construction Printing (3DCP) is a new and emerging field of additive manufacturing, predicted to revolutionise the construction industry [1]. Through automation and digital design, the need for conventional, laborious and geometrically limited cast in place concrete can be replaced. Although we are not quite at the stage of practical implementation in construction sites and the vision of robots replacing workers is still to come, research in this field has been underway for the last 10 years [2–4].

There are various methods of 3DCP using cementitious materials being developed, namely the extrusion based and powder based methods, although currently the most promising and investigated is

* Corresponding author.
E-mail address: tmarchment@swin.edu.au (T. Marchment).

https://doi.org/10.1016/j.matdes.2019.107684

the extrusion-based method [2,5–7]. Extrusion 3DCP is analogues to the fused deposition modelling (FDM) seen in polymer 3D printing [8]. Originating from the University of Southern California as "Contour Crafting", typically a high cement content, and relatively stiff mortar is pumped to a nozzle. This nozzle is fixed at the end of an automated machine where the mortar mix is then deposited. With continuous movement of the nozzle and mortar deposition, an object can be constructed with a layer by layer fabrication. [9,10].

Due to the nature of the 3DCP techniques, many new and unexplored problems arise from the machine technology, materials technology and structural performance. As the research into 3DCP is still in its early stages, many of these issues are yet to be solved. One major issue is not being able to use conventional reinforcement to provide tensile strength. Another issue is that due to the layer by layer fabrication and time gap effects, the layer interface becomes a critical position of weakness. Therefore, obtaining a strong interface bond becomes crucial in the strength of the structure itself and durability performance [2,3,11–13].

Before 3DCP there was limited research into fresh concrete to concrete adhesion, as most research focuses on the adhesion of fresh to old concrete. 3DCP brings about many new constraints and factors that can create a weak interfacial bond or often termed "cold joint" due to the lack of intermixing between layers [14]. Predominately major influencing factors are the stiffness/dryness of the deposited layer, and the time gap between successive layer depositions. When a printed layer is exposed to environmental drying effects, the interlayer strength can drop as much as 50% compared to the layer which is protected from drying [15]. As the phase change requirements of the 3D printed concrete are succumbed to shape retention and the sequential loading of fresh layers, the interlayer strength quality becomes a balancing act of the drying rate [16,17].

The theories behind the bond formation can be classified as either mechanical or chemical. Chemical bond referring to the hydration and bonding of cement particles across the interface. While mechanical bonding relies solely on the physical attributes of the layers [18]. Currently research on the 3DCP interlayer bond identifies that due to mechanical factors, localised voids at interface are apparent through microstructural analysis techniques [19–21]. These voids are a direct result of the surface roughness and the stiffness of layers being extruded. The inability of the layers to mould and anchor into the pore structure of the underlying layer therefore exhibits not only poor anchorage but reduced contact area. A study has shown that the rate of drying, to the development of voids at the interface, induce a logarithmic decrease in bond strength [22].

Therefore, to improve the bond strength due to time gap interval drying, there is a need to either decrease the void structure or increase the contact area at the interface. Improvements in tensile strength have been documented from increased contact area and interlocking, through a tongue and groove style layer fabrication [23]. Surface moisture of the layers has shown to also increase the bond strength of 3DCP elements. It is assumed the increased or maintained malleability provides mechanical anchorage into the layer atop [24]. The surface moisture in these cases was attributed to the lubrication layer (formed by the plug flow extrusion style [15]) and bleed water.

As previously mentioned, the interface bond has been characterised by common microstructural analysis techniques (primarily SEM and MIP) [19–21]. The drawbacks from these methods are that they involve damaging the sample, inducing the possibility of micro cracks at the interface, potentially causing misleading results. These techniques are also time intensive, with a minimal view of the interface (typically the cross section), without considering the bond area or void distribution longitudinally. Image analysis with X-Ray or computed tomography scans (CT) can provide a holistic view of the interface but are time consuming and costly [25].

Image analysis has been widely adopted by many fields from biomedical to materials research, as it provides a practical platform to provide visual and quantitative results. Within the field of concrete research image analysis is used for many applications such as mineralogical analysis of cements [26], damage characterisation [27], frost damage [28] and even air void determination [29]. Image analysis involves the use of software to extract objective information from images, through algorithms. Digital image acquisition is a key component in image processing, as a high-resolution image must be obtained to perform the analysis. Typically, microscopy and laser scanning are used but have limitations due to either cost or high magnification, creating an inability to obtain a complete image of the section. Image acquisition using flatbed scanners can solve these issues as a cheap alternative to provide fast and quality results [30].

Using experimental and analytical work this paper seeks to validate that a major issue in the interface bond is attributed to the mechanical properties due to layer drying and localised void structure. Through the increase of contact area at the interface it is believed a stronger bond will be obtained. Taking inspiration from bricks and mortar construction; an experimental process of applying various malleable cementitious pastes between layer depositions was adopted. Samples were fabricated with alternate colour pigments (red and white) in each layer, to further characterise the interface.

In this study attempts were made to evaluate the capability and practicality of flatbed scanner to characterise the bond and gain a quick and quantitative estimate of the entire contact area. Using a flatbed scanner on the fractured interface of pigmented layers, combined with image processing a holistic determination of the contact area or "effective bond" can be concluded.

2. Materials and methods

2.1. Materials

2.1.1. 3D printed mix

An ordinary Portland cement conforming to the Australian Standard, AS 3972 [22] general purpose (Type GP) cement was used in this study. The percentages of C_3S, C_2S, C_3A and C_4AF as the main constituents of Portland cement were 57.59%, 14.87%, 4.10% and 13.94%, respectively. Two sieve graded high silica purity sands with two different particle sizes supplied by Sibelco Pty Ltd. were used in this study. The finer silica sand denoted as "30/60" has a mean particle size of approximately 500 μm and the coarser silica sand denoted as "16/30" has a mean particle size of approximately 800 μm. The sieve analysis results were shown in Fig. 1.

The 3D printed mix was developed to primarily meet extrudability and buildability requirements which is a mixture of ordinary Portland cement (OPC), two graded sands and tap water. The mix proportions are presented in Table 1.

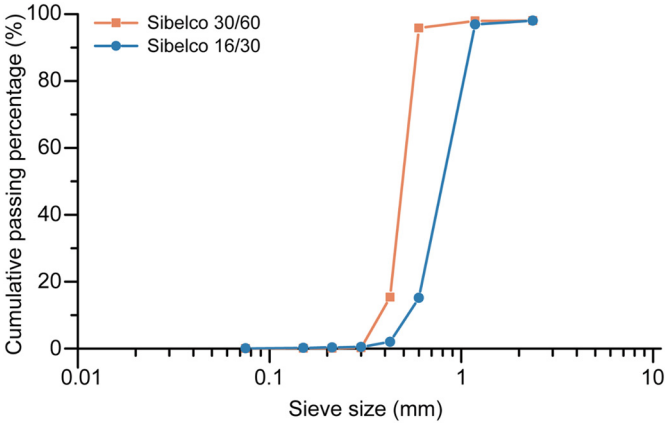

Fig. 1. Sieve analysis of the silica sands.

Table 1
Mix proportions of the 3D printed mix.

OPC	Sand (30/60)	Sand (16/30)	Tap Water	Colour Oxide
1.000	1.000	0.500	0.360	0.025

Note: All numbers are mass ratios of the OPC weight.

2.1.2. Paste mix

To strengthen the bond between the 3D printed specimens, four OPC-based paste mixtures were used as the bonding interface, like a glue, between 3D printed layers. All paste mixtures had a water to binder ratio of 0.36. The paste mixtures were developed to primarily increase the effective bond area, with a more malleable interface compared to conventional layer by layer construction. Three admixtures including retarder, viscosity-modifying agent and slump-retention agent were used in this study. These admixtures are supplied by BASF Australia. The paste mixtures also had a red colour oxide (supplied by Avista Pty Ltd.) added to distinguish from the 3D printed layers. The various pastes and mix proportions are found in Table 2.

The Paste-Control can be classified as the control paste mixture while the others are all mixed with a specific liquid admixture to increase bond strength performance. Paste-Re contains a polymer-based concrete retarder conforming to Type Re, AS1478 [31]. Primarily this additive was used to reduce the heat of hydration effects on the paste, to avoid rapid surface drying. Paste-VMA, contains a viscosity-modifying agent conforming to Type SN, AS1478 [31], used as a thickening agent to increase the viscosity and workability and reduce segregation of the paste. Paste-SP contains a chloride free, polycarbonate ether-based (PCE) superplasticiser conforming to Type SN, AS1478.1-2000 [31]. This admixture would allow greater dispersion of cement particles to give an increased workability/malleability for bond area anchorage.

2.2. 3D printing procedure

A custom-built lab scale 3D printing apparatus was used with a piston-based extrusion system. The piston extrudes the 3D printed mix through an Ø50 mm × 400 mm cylinder and out of a nozzle. The nozzle chosen had an opening of 15 mm × 30 mm to allow for a large surface contact area. The nozzle was also set at an angle of 45° to the build platform as a more consistent surface texture was observed on the extruded specimens under this arrangement. Under this arrangement, there is less vertical pressure inducing bond contact compared to the typical 90° nozzles. Rheological differences in layer depositions due to extrusion type factors, such as screw extrusion techniques versus piston extrusion, have been identified by Roussel [15].

Samples were printed in two layers at a deposition rate of 12 mm/s with the substrate layer (first layer) containing red oxide colouring and the overlay layer (second layer) containing the white oxide colouring. A time gap interval of 15 min was maintained between successive layer depositions. In the case where a cementitious paste is applied at the interlayer, a brush was used to coat a 1 mm paste layer immediately on the substrate layer after deposition. This would replicate the process of have two consecutive nozzles, one depositing the mix and the other applying the paste as shown in Fig. 2(c). The 3D printed layers in these samples contained only white oxide colouring as the paste layers were coloured red, distinguished in Fig. 2. All samples were printed in approximately 400 mm lengths and left to cure at ambient temperature (23 ± 3 °C) for 7 days in a conditioning room. The printed samples were then cut into approximately 50 mm (L) × 30 mm (W) × 30 mm (H) blocks for testing, as shown in Fig. 2(b).

2.3. Test methods

2.3.1. Flowability

To measure the flowability of the mortar mix and the paste mixtures the procedure for flow of hydraulic cement mortar ASTM C1437 was adopted on a flow table adhering to ASTM C230/C230M [32]. The flowability was measured at 3 min and 15 min after adding water and mixing. These measurements were implemented to simulate the time gap interval in the 3D printing procedure adopted in this study, and record any changes in the flow characteristics, such as stiffness.

2.3.2. Compressive strength

The 3D printed mortar and paste mixtures were cast into cube samples measuring 25 mm × 25 mm × 25 mm and subject to compressive testing after 7-day ambient curing. The samples were cured at ambient temperature (23 ± 3 °C) for 7 days. 6 cube samples of the 3D printed mix and each paste mixture were tested under a load rate of 20 ± 2 MPa/min (AS1012.9:2014) [33].

2.3.3. Interlayer bond strength

Custom made clamps with two centrically loaded pin connections were used for uniaxial tensile testing to measure the interlayer bond strength. As the tapered claws of the clamps can grip and align directly at the interlayer an even distribution of stress at this point can be achieved. As with these samples the narrow cross section at the interface prevents slippage (Fig. 3). The printed samples cut at 50 mm long sections were tested at a displacement rate of 1 mm/min after 7-day curing. A minimum of 9 samples per paste type were tested.

3. Image analysis

To gain a quantitative result of the bond area a flatbed scanner was adopted for image acquisition to perform the image analysis. Flatbed scanner has been proved to be an efficient tool for high quality image acquisition by several research works.

Peterson et al. [34] used a flatbed scanner to quantify air void characteristics from a polished concrete surface image. A series of sample treatment steps has been done to distinguish the air void from hardened cement phase and aggregates, including surface polishing, phenolphthalein solution spraying and oven drying. A “minimum distance to means” classification algorithm was used to classify all the pixels in different phases.

Le et al., [29] used a flatbed scanner to analyze the inter-filament voids distribution in 3D printed mortar specimens. Surfaces were cleaned and sprayed with a black paint. Once dry, a white paint was

Table 2
Mix proportions of the OPC-based paste mixtures.

Mix ID	OPC	Tap water	Colour oxide	Admixtures	
				Dosage	Type
Paste-control	1.00	0.36	0.25	–	–
Paste-Re[a]				0.3 ml/100 g OPC	Retarder
Paste-VMA[b]				0.9 ml/100 g OPC	Viscosity-modifying agent
Paste-SP[c]				0.3 ml/100 g OPC	Slump-retention admixture

Note: All numbers are mass ratios of the OPC weight except the admixtures.
[a] A retarder (MasterSet RT 122®) was used in this mix to reduce heat of hydration effects.
[b] A viscosity-modifying agent (MasterMatrix 362®) was used in this mix to increase flowability.
[c] A slump-retention admixture (MasterSure 1008®) was used in this mix to maintain viscosity.

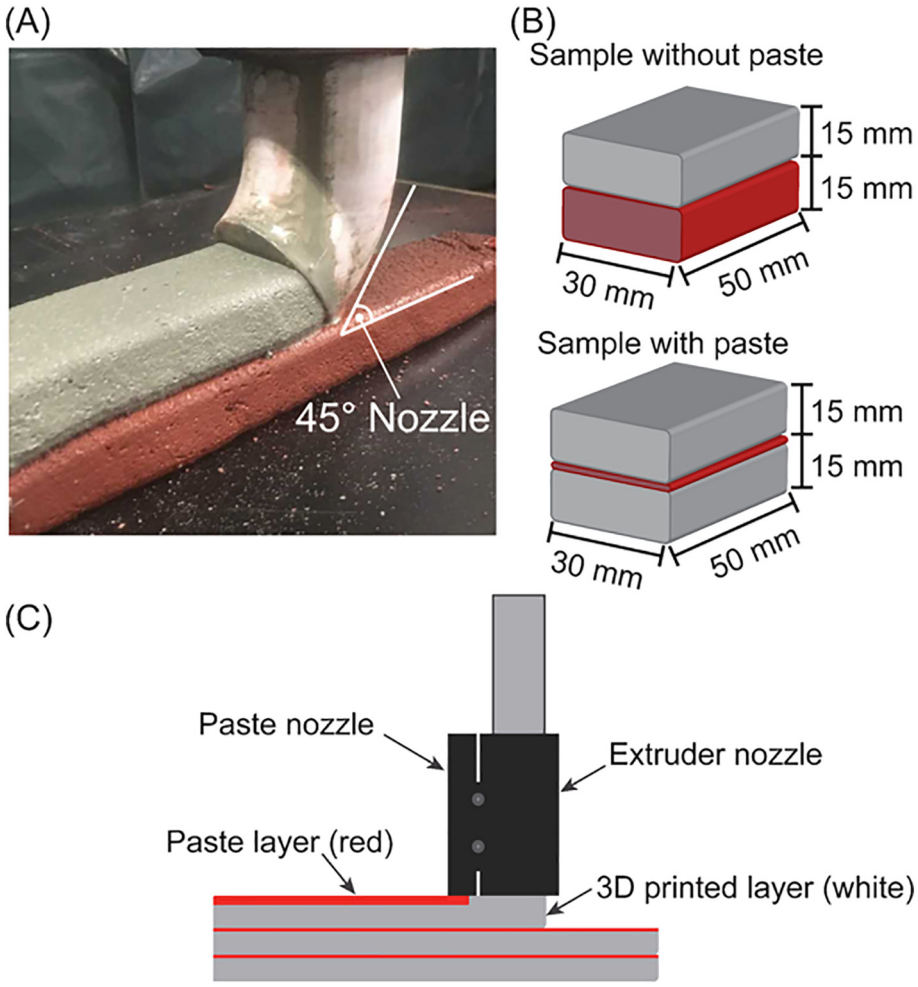

Fig. 2. (a) Mortar mix being extruded from 45° angle nozzle without a paste mixture between, (b) 50 mm (L) × 30 mm (W) × 30 mm (H) samples with and without a paste mixture applied between layers. (c) A schematic of the proposed twin nozzle extruder depositing the paste layer and 3D printed layer.

rolled on to reveal the voids that retained the black colour. The surface was subsequently scanned, and the number of voids and their area was counted by a void measuring software.

Commonly perpendicular cross sections of 3DCP elements interface are analysed to determine the void structure. This technique provides only a very small section of the interface to be analysed at one time. To gain a more holistic and quantitative representation of the void distribution, and contact area at the interlayer, longitudinal sections through the interface were analysed. The samples are fractured through the interface during tensile testing. Each layer is deposited with alternate red and white colouring as shown in Fig. 2. The fractured halves allow for the remaining pigmented deposits of the opposing layers to be visible. Clear boundaries of voids and areas of contact can be visually identified. Using fractured specimens was the preferred method compared to other researchers preparing samples by means of cutting and polishing. As the interlayer does not align perfectly level cutting and polishing would not provide a true indication of the interlayer void structure.

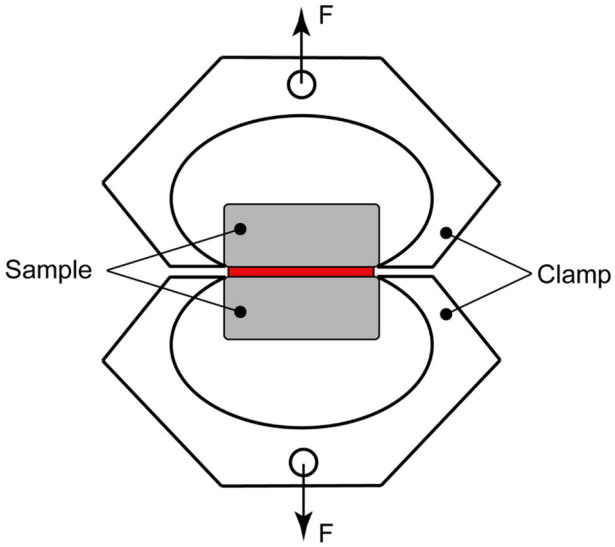

Fig. 3. Schematic illustration of the interlayer bond strength measurement.

Using colour thresholding to determine the boundaries of the pigments on each half of the specimen, correlated to the pixels within the specified spectrum, provide an indication of the contact area. This process is similar in nature and takes inspiration from Peterson et al. [35].

In this paper the resultant bond determined from the image analysis is termed “effective bond” as it is a percentage of the “nominal bond”; Nominal bond is defined as the nominal bond area of the interface dimensions. The flow diagram of the image processing methodology is described in Fig. 4.

3.1. Image acquisition of fractured surfaces

The fractured surface image of the specimen was collected from a commercially available flatbed desktop scanner (Hewlett-Packard®

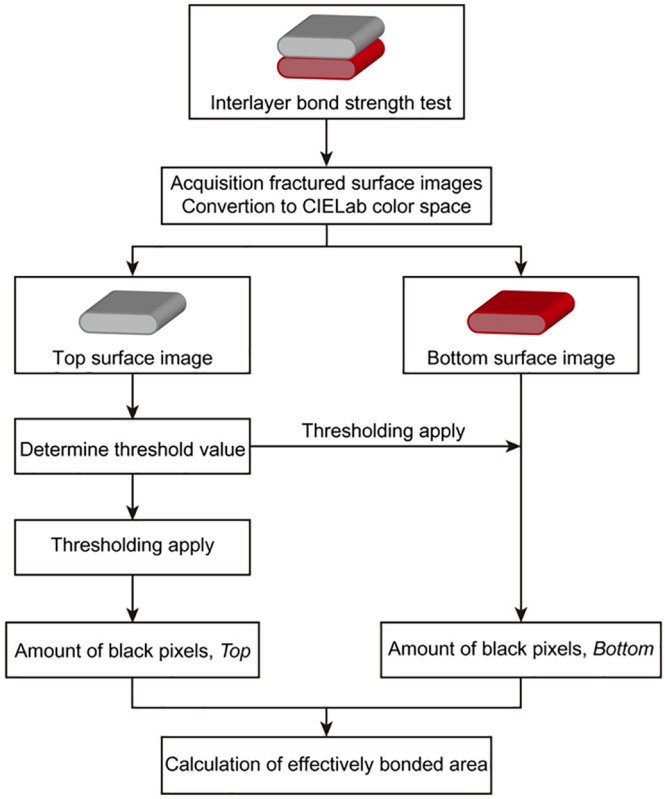

Fig. 4. Flow diagram of the methodology of calculating the effectively bonded area.

Scanjet G3010), which has a maximum optical resolution of 4800 × 9600 dpi. The flatbed scanner employs a charged coupled device (CCD) image sensor and operates in reflectance mode. A schematic of the scanning procedure is illustrated in Fig. 5(a). The sample to be scanned was placed in the centre of the glass plate and was covered so it was isolated from external light. The scan head, which consists of mirrors, filters and a CCD sensor, moved under the glass plate by a stepper motor. Image of the scanned sample was reflected onto the CCD sensor by several mirrors.

The images were scanned at a resolution of 1200 dpi by using software bundled with the scanner. All automatic correction and enhancement functions were disabled to ensure the raw image was not manipulated. The edges of the scanned images were then manually removed by using the bundled software. It should be noted that the cropped top surface and bottom surface images from the same specimen had identical sizes (same number of total pixels). The image was then saved as 24-bit Tagged Image File Format (tiff) file. The scanned images are shown in Fig. 5(b).

3.2. Detection of effective bond area

This proposed method used CIELab thresholding which defines a region in each colour space, in such a way that all the pixels that fall into this region are treated as effectively bonded area. When looking at colour as a potential feature, the RGB format is not always optimal, mainly because the brightness information of each pixel is directly linked to the colour information. CIELab is a colour space described in three dimensions of the coordinates L*, a*, b*, where: L* is lightness and a* and b* are chrominance components. CIELab space has been more perceptually uniform than other colour spaces. For this reason, the scanned images were converted from RGB to CIELab before the thresholding process.

To determine whether the thresholding method that has been carried out is successful or not, it relies solely on human intervention. Therefore, the threshold value needs to be manually varied until acceptable results are achieved, based on the human observation. Acceptable results refer to a visual determination of the threshold that overlays most accurately with the observed contact area on scanned fractured

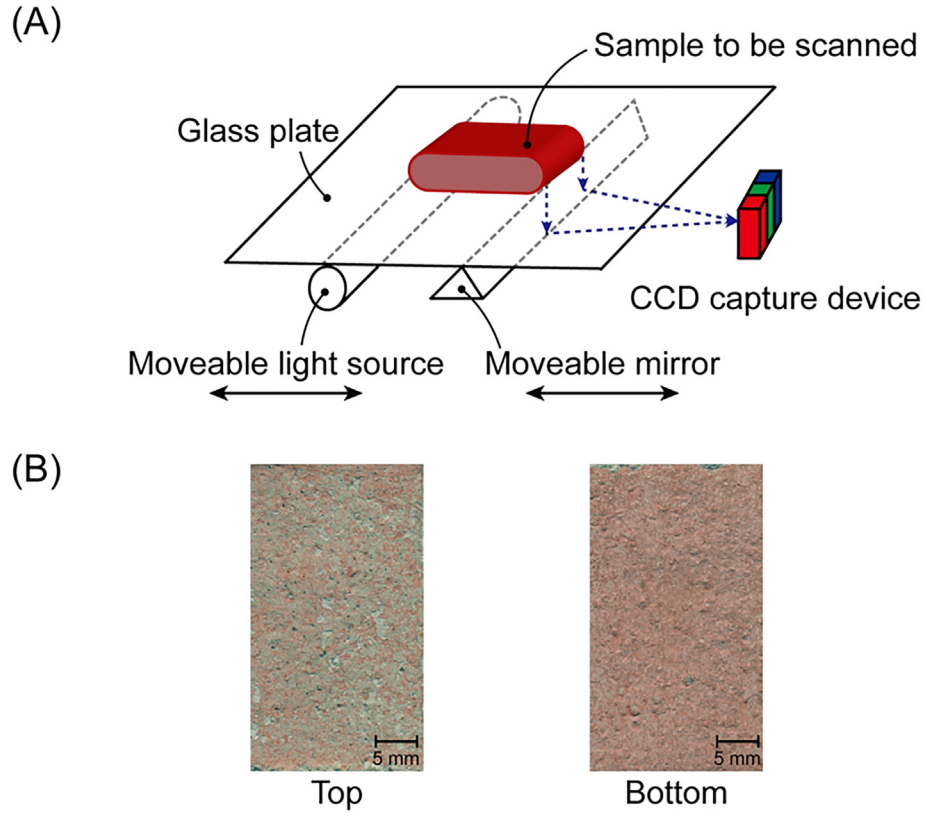

Fig. 5. (a) Schematic illustration of the scanning procedure. (b) Scanned images of fractured surfaces.

samples for each sample group. The thresholding process was carried out by using MATLAB® Image Processing Toolbox. The optimal threshold values for each group of specimens are listed in Table 3. Fig. 6 shows the result after applying the colour thresholding on the scanned image.

3.3. Calculation of effective bond area

After the CIELab thresholding being applied on the scanned image, the amount of the black pixels on both images were used to calculate the effective bond area.

It should be noted this calculation is based on the following assumptions:

1. The black pixels on the top image is considered as completely bonded area.
2. The paste applied is considered to adhere completely to the bottom layer.

The effectively bonded area ratio is calculated from Eq. (1):

$$\textit{Effective Bond Area}\ (\%) = \frac{\textit{Total} - (\textit{Bottom} - \textit{Top})}{\textit{Total}} \times 100\% \quad (1)$$

where: *Total* is the total amount of pixels; *Bottom* is the number of black pixels of the bottom image; *Top* is the number of black pixels of the bottom image.

4. Results and discussion

4.1. Flowability

To idealise and approximate the flow characteristics of the 3D printed mix and paste mixtures flow table tests conforming to ASTM C1437 were performed. Spread diameter measurements of samples after 3 min and 15 min of initial water addition were taken, with a fresh mixture used in each test. This procedure was undertaken to replicate the application of a paste layer on the substrate layer, with a 15 min time delay, before the overlay layer is deposited. Correlations between flow characteristics pre and post application were assessed. The results for this test are shown in Fig. 7.

The 3D printed mix, as expected proved to have the highest resistance to flow. A difference of 15 mm was observed between the 3 min and 15 min tests at spread diameters of 166 mm and 151 mm. Comparing the paste mixtures and considering the accuracy of the testing regime, spread diameter results are comparable. All the paste mixtures are significantly more flowable than the mortar mix at 3 min and 15 min, ranging above 200 mm.

The Control paste shows a significantly higher rate of stiffening between 3 min and 15 min at a 30 mm spread diameter. As the 15 min spread diameter of 184 mm was recorded for the Control paste, it can also be identified as the stiffest paste mixture at the time of application. Paste mixtures Re, VMA and SP contain cement admixtures are observed to have minimal, if not slightly increased flow properties. Paste SP exhibits the largest spread diameters with an increase (as opposed to decrease in other mixes) in flowability after 15 min from 226 mm to 230 mm. This is likely to have been caused by the activation and diffusion of cement particles due to the mix containing a PCE. As this paste contained a superplasticiser there would be a desperation of cement particles, therefore this phenomenon is explainable.

It can be concluded from the test that the addition of admixtures in the pastes will increase or maintain the flow and malleability properties over a 15 min period. As can also be observed, the Control paste mixture does have comparable 3 min flow characteristics, it does decrease within the 15 min time gap period far greater than the other mixtures.

Table 3
Optimal threshold values for each group of specimens.

Specimen ID	Optimal threshold values		
	L*	a*	b*
No paste	[36.157, 71.050]	[5.796, 29.140]	[10.541, 29.272]
Paste-Control	[44.994, 68.017]	[1.172, 24.660]	[5.038, 25.522]
Paste-Re	[36.808, 61.186]	[5.309, 26.169]	[4.185, 31.514]
Paste-VMA	[32.298, 64.060]	[2.217, 23.028]	[8.153, 31.435]
Paste-SP	[42.876, 62.856]	[9.476, 30.418]	[13.084, 29.932]

Note: L* is lightness, a* and b* are chrominance components in CIELab colour space.

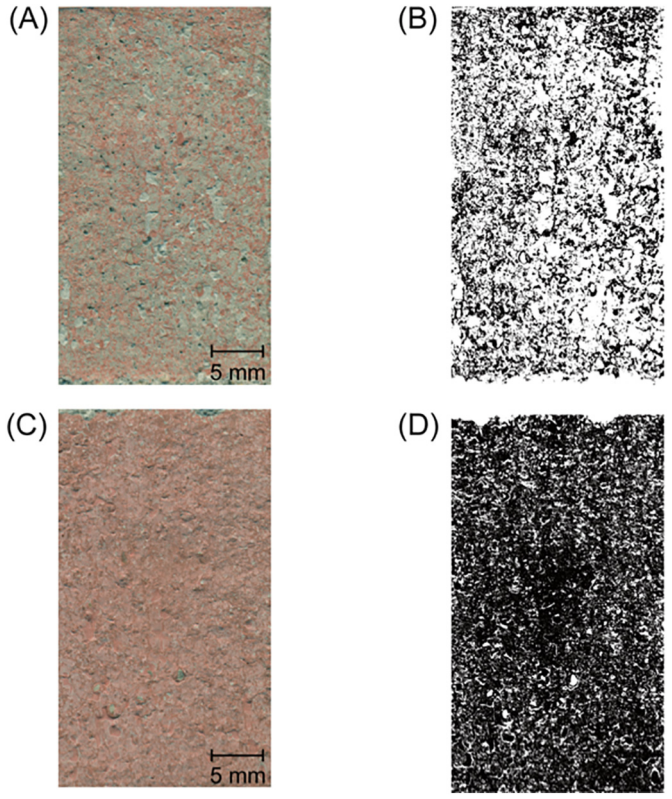

Fig. 6. Results of application of colour thresholding. (a) Top Image before thresholding, (b) Top Image after thresholding, (c) Bottom Image before thresholding, (d) Bottom Image after thresholding.

4.2. Compressive strength

To maintain consistency and prevent variations in strength development, the W/C ratio of 0.36 was maintained from the 3D printed mix

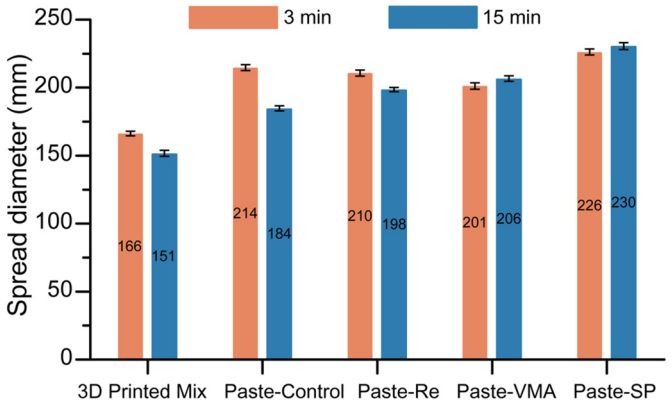

Fig. 7. Flowability test results for the 3D printed mix and paste mixtures. Note: the numerical values indicate the spread diameter measured after dropping 25 times.

through to the paste mixtures. Cast cube samples of each mixture were tested in compression at 7 days. Fig. 8 shows the compressive strength results of the mixtures, with the error bars indicating the mean ± standard deviation. The presented data indicates that 3D printed mix has the lowest average compressive strength of 34 MPa. The most likely cause of lower strength in the 3D Printed Mix is due to the addition of sand, as the paste mixtures have a higher cement content. The Control paste, Paste Re and Paste VMA exhibited a higher average compressive strength ranging from 42.1 MPa to 45.5 MPa. Paste SP is noted to have the highest average compressive strength of 53.4 MPa, which can be attributed to the particle dispersion of cement associated with superplasticiser.

A comparative indirect analysis of the compressive and interlayer bond strength is conducted. The analysis is done on the basis that the compressive and tensile strengths are strongly correlated. The 3D printed mix will have an inherently lower interlayer bond capacity therefore, samples fabricated with no paste applied at the interlayer, we must factor this difference and contact area.

4.3. Inter-layer bond strength

Test specimens were subjected to uniaxial tensile testing to measure interlayer bond strength, and the test results are presented in Fig. 9. The conventionally fabricated samples with no paste layer yielded an average interlayer strength of 0.27 MPa. The Control paste samples produced slightly higher average interlayer strength of 0.30 MPa. Paste-Re and Paste-VMA both exhibit an average interlayer strength of 0.34 MPa. Most notably Paste SP was observed to yield the highest average interlayer strength of 0.43 MPa. All samples were observed to have a uniform fracture at the interlayer, with fracture occurring between the overlay layer and top of paste layer. Therefore, on the interface that is exposed to surface drying the longest.

Despite the standard deviations of the interlayer strength results are higher than the compressive strengths, a clear trend can be observed. The data indicates that the addition of a paste layer does provide an increase in interlayer strength. Initially addition of the Control paste, shows an 11% interlayer bond increase. The addition of pastes containing additives shows and interlayer strength increase of 26% to a 59%. The highest increase was observed with the addition of superplasticiser. These results replicate similar trends observed in the flowability and compressive strength tests.

4.4. Effective bond area

Using the image processing methodology of the fractured samples described in Section 3, an estimate of the effective bond area for each grouping was calculated against the nominal area. The average results are shown in Fig. 10. The standard deviations of these results were

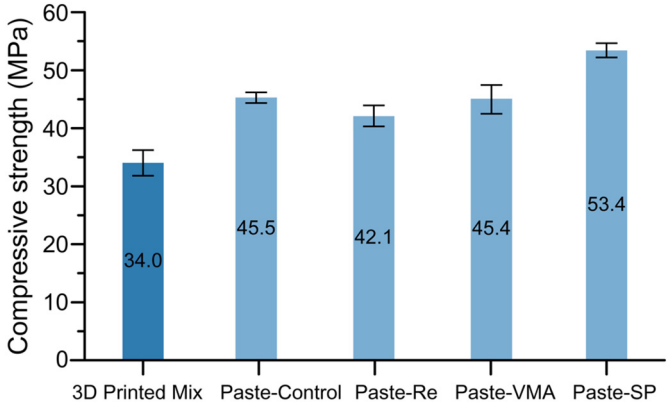

Fig. 8. Compressive strength results of the 25 mm × 25 mm × 25 mm cast cube samples. Note: the numerical values indicate the average compressive strength.

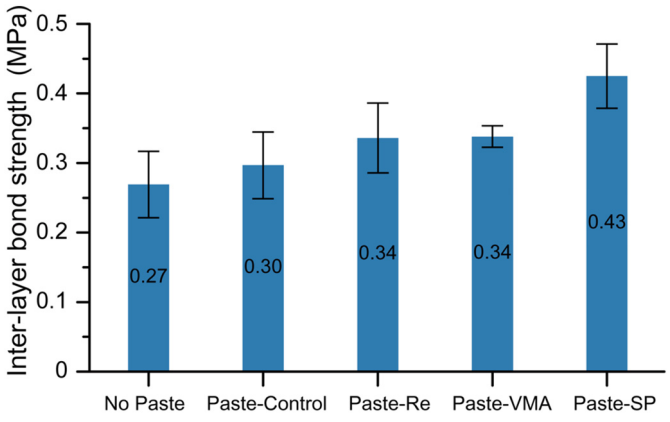

Fig. 9. Interlayer bond strength test results from uniaxial direct tensile test. Note: the numerical values indicate the average inter-layer bond strength.

very small ranging between 0.02 and 0.03 for each paste type grouping. The Control paste is observed to have the lowest effective bond area of 0.38. These results being lower than the No Paste result of 0.68 at first seemed to contradict the main hypothesis of these trials being the malleability of the substrate layer. However, this is likely to be due to the observed dryness of the surface after the 15 min time gap interval compared to the other paste mixtures, minimising the ability to penetrate pore structure of the overlay layer. Similarly, the VMA samples attained an effective bond area of 0.60; despite the observation that this paste is the most viscous of the paste mixtures. The samples with no paste between layers were measured to have an effective bond area of 0.61. On the upper end of the spectrum, Paste-Re exhibited the highest effective bond area of 0.85, followed by Paste-SP at 0.80. Each of these pastes having different attributes, namely, Paste-Re having extended setting time, Paste-VMA having high viscosity and Paste-SP having high flowability give us directions to elucidate the type of attributes which are important for improving the bond strength.

4.5. Discussion bond area vs interlayer bond strength

From the interlayer strength results described previously there was a trend of increasing strength with the application of a paste. To consolidate the validity of these results, interlayer strength results presented from similar works [36] are compared as the same mix composition was used, except there was no addition of colour pigment. This interlayer strength data, although of a higher magnitude, demonstrate that these paste mixtures increase the bond strength. The two data sets were shown in the same plot to validate the trend further. This data is presented in Fig. 11 with the interlayer strength results obtained in

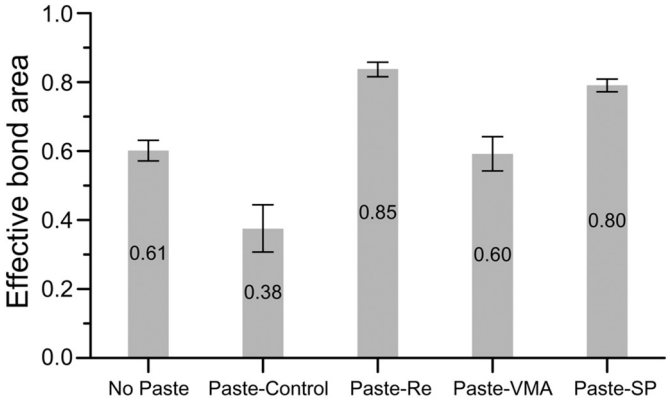

Fig. 10. Effective bond area of each sample type.

this paper defined as 'Mix 1', while the previous data set is defined as 'Mix 2'.

To directly compare the effect of bond area on interlayer strength, results from Figs. 10 and 11 are combined in Fig. 12. As not all the samples shown in Fig. 11 were not subject to the image analysis procedure to determine bond area, results are plotted assume that all samples display the effective bond area relevant to the paste type employed.

From Fig. 12 a common trend is observed for Mix 1 and Mix 2, relating the effective bond area and the interlayer strength. A direct correlation to the effective bond area and interlayer strength of samples applied with a paste mixture is evident. Amongst these samples the higher the effective bond area, the stronger the bond.

This trend is not analogues to the No Paste samples, the No Paste samples do display a higher effective bond area than the Control paste and an equivalent bond area to the VMA paste samples. Although the No Paste samples do have an overall lower interlayer strength than the other samples. This can be explained with the lower compressive strength of the material in comparison to the paste mixtures (Fig. 8).

The Control paste is identified as having the lowest effective bond area and the Paste-VMA, which is comparable with the No Paste samples at approximately 0.60. Although they both have similar compressive strengths, an explanation can be drawn to the significantly low associated effective bond area between them. It is noted that from flow tests the Control paste had the highest rate of stiffening after the 15 min time gap. It was also observed during the fabrication phase that there was noticeably high level of dryness of the surface of the Control paste after the 15 min time gap. It can be assumed that the heat of hydration produced in this paste has accelerated the evaporation of the surface moisture. Sanjayan et al. [24] identified that the moisture level at the surface between the layers had a large impact on bond strength. VMA admixtures have an increased dynamic viscosity and are highly hydrophilic, binding the water molecules to increase volume and water retention [37]. As the VMA paste, does increase the viscosity of the mixture, identified in the flow table test, it was similarly observed to have less of a surface drying effect than the Control paste in the deposition phase.

Likewise, the effect of the retarder in the Re paste reduces the heat of hydration of cement within the paste [38]. As such, a retention of the surface moisture of the paste occurs resulting in a higher bond strength. This phenomenon can also be linked to the SP paste, although a reduction in the heat of hydration is not to the same extent of the Re paste. The greater interlayer strength in SP paste can be attributed to the higher compressive strength and flow properties due to greater particle dispersion by the action of superplasticisers [39].

The initial hypothesis was that the higher flowability of the paste mixtures would allow for a greater malleable surface area, in turn creating a greater effective bond area. However, from observation within this

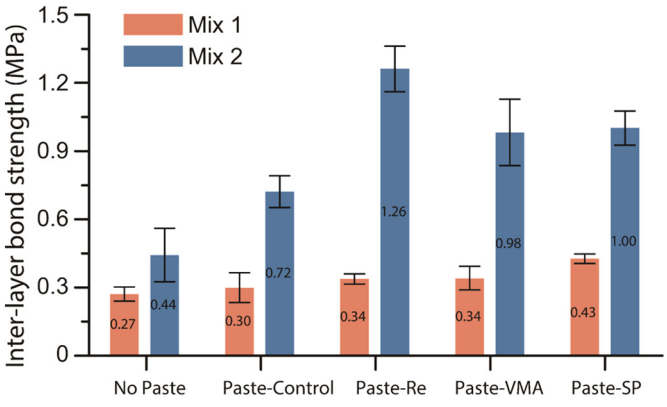

Fig. 11. Interlayer bond strength results. Note: Mix 1 = mix presented in this paper; Mix 2 = results from Marchment [36] (same mix composition as Mix 1 except without colour pigments).

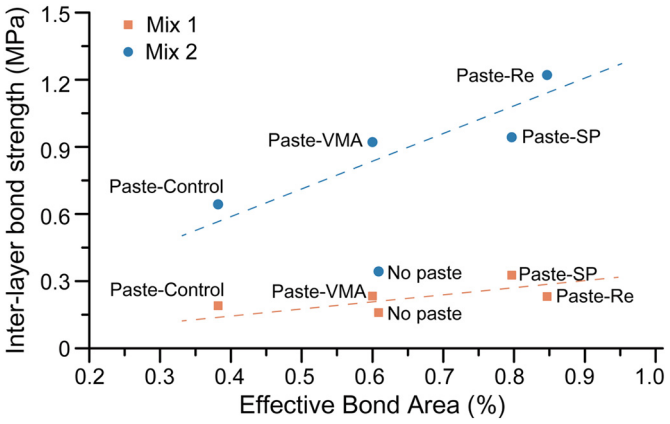

Fig. 12. Interlayer bond strength versus the effective bond area. Note: Mix 1 = mix presented in this paper; Mix 2 = results from Marchment [36] (same mix composition as Mix 1 except without colour pigments).

study and the correlation from the work of Sanjayan et al. [24], it not necessarily the malleability of the paste but the surface moisture effects on the bond strength. This is affected by factors such as the migration of cement particles into the overlay layer, and possible capillary suction.

5. Summary and conclusions

The interface of mortar 3D printed layers are considered a critical point of weakness due to either mechanical or chemical factors. Taking inspiration form bricks and mortar construction, various cementitious pastes were deposited between the layers, with the intention to enhance the mechanical anchorage and minimise localised voids at the interface. Application of this paste layer was performed with a brush although an autonomous deposition could be employed. Layers were deposited with opposing colour schemes to be able to perform an image analysis on the fractured samples. Through this study the following conclusions can be drawn;

1. Application of a paste layer with higher and sustained flow characteristics increases the bond strength of layers compared to layers conventionally manufactured.
2. A unique method of quantifying the effective bond area with colour addition to the layers, flatbed scanning, and an image processing analysis was applied and proven to provide reliable and consistent results.
3. A strong relationship between effective bond area and the interlayer strength exists.
4. The bond area in the samples with pastes applied are strongly attributed to the stiffening effects and surface moisture (or dryness). This proves to be a critical factor in addition to the effective bond area, as evidenced by No-Paste samples.

The assumption at first was that the higher flowability of the paste mixtures would allow for a greater malleable surface area, in turn creating a greater effective bond area. However, through this study further evidence is produced to suggest that it is not only the flowability/malleability of the paste which is critical, but the surface moisture retention is also another critical factor. The effects of this may be lack of moisture decreasing the degree of hydration and lowering of strength.

Further research is needed to be undertaken to understand the relationship of the surface moisture and bond attributions at the interface. An in-depth understanding of the surface characteristics and their relationship to bond strength can help in designing the 3D Construction Printing. It should be noted that it is not always necessary to have an intermediate paste layer to benefit from this research. It is known that the outer layer of extruded layers, known as lubrication layer, has different

properties to the rest of the concrete. It is possible to manipulate the properties of this lubrication layer so that the desirable outcomes can be achieved.

Author contributions

Taylor Marchment is the primary author of the paper. He conceptualised, investigated and performed the testing, hypothesis, writing data curation and formulation of the methodology of the study. Jay Sanjayan is the supervisor and secondary author of this paper, whom also provided conceptualisation, validation, editing and hypothesis of the paper. Ming Xia is the third author of this paper whom provided programing and created analysis software while also writing and providing visualisation of figures and tables throughout the paper.

Acknowledgements

The authors gratefully acknowledge the Australian Research Council funding (DP170103521, LE170100168) for this work.

References

[1] Wangler, T., et al., Digital Concrete: Opportunities And Challenges. RILEM Technical Letters, 2016. 1: P. 67.
[2] R.A. Buswell, et al., 3D printing using concrete extrusion: a roadmap for research, Cem. Concr. Res. 112 (2018) 37–49.
[3] G. De Schutter, et al., Vision of 3D printing with concrete — technical, economic and environmental potentials, Cem. Concr. Res. 112 (2018) 25–36.
[4] Nematollahi, B., M. Xia, and J. Sanjayan. *Current Progress Of 3D Concrete Printing Technologies*. In *ISARC. Proceedings Of The International Symposium On Automation And Robotics In Construction*. 2017. Vilnius Gediminas Technical University, Department Of Construction Economics & Property.
[5] S.H. Bong, Al Et, Fresh And Hardened Properties Of 3D Printable Geopolymer Cured In Ambient Temperature, Springer International Publishing, Cham, 2019 3–11.
[6] Xia, M., B. Nematollahi, And J. Sanjayan. Compressive Strength And Dimensional Accuracy Of Portland Cement Mortar Made Using Powder-Based 3D Printing For Construction Applications. 2019. Cham: Springer International Publishing: p. 245–254.
[7] M. Xia, B. Nematollahi, J. Sanjayan, Printability, accuracy and strength of geopolymer made using powder-based 3D printing for construction applications, Autom. Constr. 101 (2019) 179–189.
[8] H.-M. Zhao, Al Et, Inclined layer printing for fused deposition modeling without assisted supporting structure, Robot. Comput. Integr. Manuf. 51 (2018) 1–13 Supplement C.
[9] Khoshnevis, B., et al., *Mega-Scale Fabrication By Contour Crafting*. Int. J. Ind. Syst. Eng., 2006. 1(3): p. 301–320.
[10] R. Duballet, O. Baverel, J. Dirrenberger, Classification of building systems for concrete 3D printing, Autom. Constr. 83 (2017) 247–258.
[11] V.N. Nerella, et al., Inline quantification of Extrudability of cementitious materials for digital construction, Cem. Concr. Compos. 95 (2019) 260–270.
[12] Rushing, T.S., et al., *Investigation Of Concrete Mixtures For Additive Construction*. Rapid Prototyp. J., 2017. 23(1): p. 74–80.
[13] Marchment, T., et al., *Chapter 12 - Interlayer Strength of 3D Printed Concrete*: *Influencing Factors and Method of Enhancing*, in *3D Concrete Printing Technology*, J.G. Sanjayan, A. Nazari, and B. Nematollahi, Editors. 2019, Butterworth-Heinemann. p. 241–264.
[14] N. Roussel, F. Cussigh, Distinct-layer casting of SCC: the mechanical consequences of thixotropy, Cem. Concr. Res. 38 (5) (2008) 624–632.
[15] N. Roussel, Rheological requirements for printable concretes, Cem. Concr. Res. 112 (2018) 76–85.
[16] A. Perrot, D. Rangeard, A. Pierre, Structural built-up of cement-based materials used for 3D-printing extrusion techniques, Mater. Struct. 49 (4) (2015) 1213–1220.
[17] L. Reiter, et al., The role of early age structural build-up in digital fabrication with concrete, Cem. Concr. Res. 112 (2018) 86–95.
[18] B. Zareiyan, B. Khoshnevis, Interlayer adhesion and strength of structures in Contour Crafting - Effects of aggregate size, extrusion rate, and layer thickness, Autom. Constr. 81 (2017) 112–121.
[19] J. Van Der Putten, G. De Schutter, K. Van Tittelboom, The Effect Of Print Parameters On The (Micro)Structure Of 3D Printed Cementitious Materials, Springer International Publishing, Cham, 2019 234–244.
[20] V.N. Nerella, S. Hempel, V. Mechtcherine, Micro-and macroscopic investigations on the Interface between layers of 3D-printed cementitious elements, Proceedings of the International Conference on Advances in Construction Materials and Systems, 3–8. 9. 2017, 2017.
[21] V.N. Nerella, S. Hempel, V. Mechtcherine, Effects of layer-Interface properties on mechanical performance of concrete elements produced by extrusion-based 3D-printing, Constr. Build. Mater. 205 (2019) 586–601.
[22] Y.W.D. Tay, et al., Time gap effect on bond strength of 3D-printed concrete, Virtual And Physical Prototyping (2018) 1–10.
[23] B. Zareiyan, B. Khoshnevis, Effects of interlocking on interlayer adhesion and strength of structures in 3D printing of concrete, Autom. Constr. 83 (2017) 212–221.
[24] J.G. Sanjayan, et al., Effect of surface moisture on inter-layer strength of 3D printed concrete, Constr. Build. Mater. 172 (2018) 468–475.
[25] W. Tian, N. Han, Pore characteristics (>0.1 mm) of non-air entrained concrete destroyed by freeze-thaw cycles based on CT scanning and 3D printing, Cold Reg. Sci. Technol. 151 (2018) 314–322.
[26] S. Ma, et al., Alite-Ye'elimite cement: synthesis and mineralogical analysis, Cem. Concr. Res. 45 (2013) 15–20.
[27] J. Valença, et al., Automatic crack monitoring using photogrammetry and image processing, Measurement 46 (1) (2013) 433–441.
[28] Z. Wang, et al., Characterizing frost damages of concrete with flatbed scanner, Constr. Build. Mater. 102 (2016) 872–883.
[29] T.T. Le, et al., Hardened properties of high-performance printing concrete, Cem. Concr. Res. 42 (3) (2012) 558–566.
[30] D. Miriello, G.M. Crisci, Image analysis and flatbed scanners. A visual procedure in order to study the macro-porosity of the archaeological and historical mortars, J. Cult. Herit. 7 (3) (2006) 186–192.
[31] AS1478, AS1478 - Chemical Admixtures For Concrete, Mortar and grout—Admixtures for concrete, Standards Australia, 2000.
[32] C. ASTM, Standard Test Method For Flow Of Hydraulic Cement Mortar. C 1437, 2007.
[33] AS1012.9, AS1012.9 - methods of testing concrete compressive strength tests-concrete, Mortar and Grout Specimens, 2014.
[34] K. Peterson, et al., Hardened concrete air void analysis with a flatbed scanner, Concrete 2001 (1775) (2001) 36–43.
[35] K. Peterson, et al., Methods for threshold optimization for images collected from contrast enhanced concrete surfaces for air-void system characterization, Mater. Charact. 60 (7) (2009) 710–715.
[36] Marchment, T. and J. Sanjayan. Method Of Enhancing Interlayer Bond Strength In 3D Concrete Printing. 2019. Cham: Springer International Publishing: p. 148–156.
[37] C. Brumaud, et al., Cellulose ethers and water retention, Cem. Concr. Res. 53 (2013) 176–184.
[38] D. Marchon, R. Flatt, Impact of chemical admixtures on cement hydration, Science and Technology of Concrete Admixtures, Elsevier 2016, pp. 279–304.
[39] G. Gelardi, et al., Chemistry Of chemical admixtures, Science And Technology Of Concrete Admixtures, Elsevier 2016, pp. 149–218.